Climate Change Projections of Severe Weather Environments by Synoptic Patterns in GFDL-CM3

SOFIA AVILA*

National Weather Center Research Experiences for Undergraduates Program, Norman, Oklahoma, and Virginia Polytechnic Institute and State University, Blacksburg, Virginia

KIMBERLY A. HOOGEWIND

Cooperative Institute for Severe and High-Impact Weather Research and Operations, University of Oklahoma, Norman, OK, and NOAA/OAR/National Severe Storms Laboratory, Norman, OK

HAROLD E. BROOKS

NOAA/OAR/National Severe Storms Laboratory, Norman, OK, and School of Meteorology, University of Oklahoma, Norman, OK

ABSTRACT

The research on impacts of climate change on severe weather has mostly focused on estimating changes of environmental parameters (e.g., convective available potential energy, deep-layer shear) in global climate models, however, this approach does not take into account the synoptic pattern that can indirectly influence severe weather. Using a self-organizing map, a type of artificial neural network, sixteen distinct synoptic patterns based on 500 hPa geopotential height anomalies are identified. Changes in daily pattern frequencies are assessed within the Geophysical Fluid Dynamics Laboratory Climate Model v3 under future representative concentration pathways (RCP) scenario, RCP4.5 and RCP8.5. Environmental parameters commonly related with severe weather environments are associated with each synoptic pattern type, and the changes of the parameters under those patterns are evaluated within the future simulations. In both RCP4.5 and RCP8.5, western/central U.S. ridge patterns are projected to become more frequent, especially during the summer, and most distinctly in RCP8.5. However, this synoptic pattern is typically unfavorable for severe weather for the U.S. as a whole. Within these patterns, convective available potential energy (CAPE) and the magnitude of convective inhibition (CIN) increase significantly, particularly in the central U.S. The increase in CIN, as well as declining frequencies in other summer patterns, could explain the overall projected decrease severe weather environment days by 2100 during JJA in RCP8.5., but there is still uncertainty as global climate models generally conflict in their projections of environmental parameters during the summer months.

1. Introduction

Severe convective storms (SCSs) are storms that produce damaging winds greater than 58 mph, hail greater than 1 inch, and/or a tornado, and are a major threat to life and property each year in the United States. SCSs have produced 160 $1 billion disaster events from 1980-2022, with an estimated total of $365.3 billion dollars ($8.5 B per year). SCSs are also the third deadliest weather disaster, resulting in 1,980 fatalities from 1980–2022 (NOAA 2022). Because SCSs pose a great danger to the population, it's important to study their change of frequency in relation to a warming climate.

Increasing SCS report frequency has many nonmeteorological influences which render the U.S. storm database impractical for use in assess trends, and disagreements between climate models representation of favorable SCS environments make it harder to find a significant correlation (Kunkel et al. 2013). Investigating changes in favorable SCS environments using an "ingredients-based" approach has been the most prevalent form of studying climate variability of potential SCSs, and environmental parameters favorable for SCS development are well-established which. This approach analyzes changes in moisture, instability, and the magnitude of deep-layer vertical wind shear in global climate model projections (e.g., Diffenbaugh et al. 2013; Trapp et al. 2007). However, the "lifting" mechanism needed for storm initiation is difficult to assess due to the relatively coarse resolution of global climate models. High-resolution simulations that permit

*Corresponding author address: Sofia Avila, Virginia Tech, Blacksburg,VA 24060)
E-mail: savila@vt.edu

convection can provide further insight (e.g., Gensini and Mote 2014, 2015; Hoogewind et al. 2017), but are expensive to produce. Parameters such as convective available potential energy (CAPE) and 0–6 km shear (S06), are more easily assessed from global climate models (GCMs). Convective available potential energy (CAPE) has a relationship to low-level temperature and moisture (i.e., specific humidity, Chen et al. 2020), and increased air temperatures allow for greater moisture (Clausius-Clapeyron relationship),such that temperature/moisture increases result in greater CAPE (Chen et al. 2020) with numerous climate projections agreeing in this aspect (Hoogewind et al. 2017). However, studies also show the magnitude of convective inhibition (CIN; the energy needed to lift an air parcel to where it becomes positively buoyant) is projected to increase, mostly over land (Chen et al. 2020), which can suppress storm development.

In the contiguous United States (CONUS), projections of CAPE have demonstrated a robust increase for all seasons, however, S06 experiences notable decreases varying by region and season which can be attributed to decreases in the meridional temperature gradient, most prominent during the summer season (Diffenbaugh et al. 2013). Furthermore, previous results indicate the most favorable SCSs environments are a result of high CAPE and high shear (Trapp et al. 2007), thus a decrease in shear could affect storm organization. However, by combining daily maximum product of CAPE and S06, Diffenbaugh et al. (2013) found that the number of severe weather days is not impacted by decreased S06, as decreases in S06 occur when there is also low CAPE. 0–1 km shear (the magnitude of the vector wind difference between the surface wind and 1-km) has been shown to be an important ingredient in supercells and tornado formation (Thompson et al. 2003). However, high-CAPE and weak low-level shear combinations are projected to increase at a higher fraction (Diffenbaugh et al. 2013).

Although the ingredients-based approach is important in our understanding of SCS-favorable environments, it does not account for storm initiation. High resolution convection-permitting model simulations can help to account for the issue, allowing the model to develop the relationship between the environment and event. While these simulations allow for convection to develop, they still cannot resolve the hazards associated with SCSs, and proxies are required to estimate their occurrence. Common proxies include updraft helicity (UH) (Robinson et al. 2013; Trapp et al. 2011) and maximum upward vertical velocity in the lowest 400 hPa (UVV) (Hoogewind et al. 2017). UH measures a storm's rotation in the updraft , and UVV measures the updraft speed within a thunderstorm. However, UH fails to replicate SCS days well during the summer season in the eastern U.S. relative to UVV, likely due to severe weather produced by more disorganized modes of convection (Hoogewind et al. 2017). Hoogewind et al. (2017) found that, generally, there is an increase in SCS frequency relative to an increase in warming, however, during the summer season, the conditional probability of SCS given favorable environmental conditions decreases. Dynamical downscaling approaches have been an effective way to study the "initiation" problem, but its computational requirements limit the ability to produce ensembles. Using synoptic patterns to project future SCS-favorable conditions has not been researched as extensively as the ingredients-based approach. It has limitations based on the assumption that synoptic variables (such as 500 hPa geopotential height) will create the environments needed for storms (Lee 2012). However, synoptic patterns are generally more reliably reconstructed in GCMs. Lee (2012) analyzed changes in 500 and 700 hPa geopotential heights, and 850 hPa temperatures, as the heights in these two pressure levels represent trough/ridge patterns and shortwave patterns as well. Warm temperature advection at 850 hPa is a good indicator of surface convergence, which might signal favorable environments. Lee (2012) used several statistical methods (principal component analysis, cluster analysis, and discriminant function analysis) to group similar patterns associated with F2+ tornado days. Two global climate models with two different warming scenarios were used to project changes in the probability of tornado day frequency during the 2050s and 2090s. The results suggested that tornado days will likely increase in the earlier part of the tornado season in comparison to other months, especially in the highest warming scenario in the 2090s. Apart from tornadoes specifically, only regional synoptic pattern analysis has been done to analyze their influence on surface conditions (e.g., Hope 2006) (e.g., Hope 2006 examined rainfall in Australia, not severe weather), and a synoptic climatology associating severe weather outbreaks in the CONUS has been built (e.g., Johns 1984), however, a warming climate provides another perspective to consider.

This study aims to combine the environmental and pattern approach to find a connection and assess how changing synoptic patterns may influence changes in SCS favorable environments under future radiative-forcing scenarios. By linking these two approaches, we hope to provide some indirect insight on the storm initiation problem.

2. Data and Methods

In this study, we will be using the Geophysical Fluid Dynamics Laboratory Climate Model v3 (GFDL-CM3), as it has shown to be a high-performing GCM in simulating the climatology SCS environments (Seeley and Romps, 2014). The simulations were produced for the Coupled Model Intercomparison Project Phase 5 (CMIP5); specifically, we will use the historical simulation (1971—2005) and two future warming experiments (2006-–2100). The representative concentration pathway

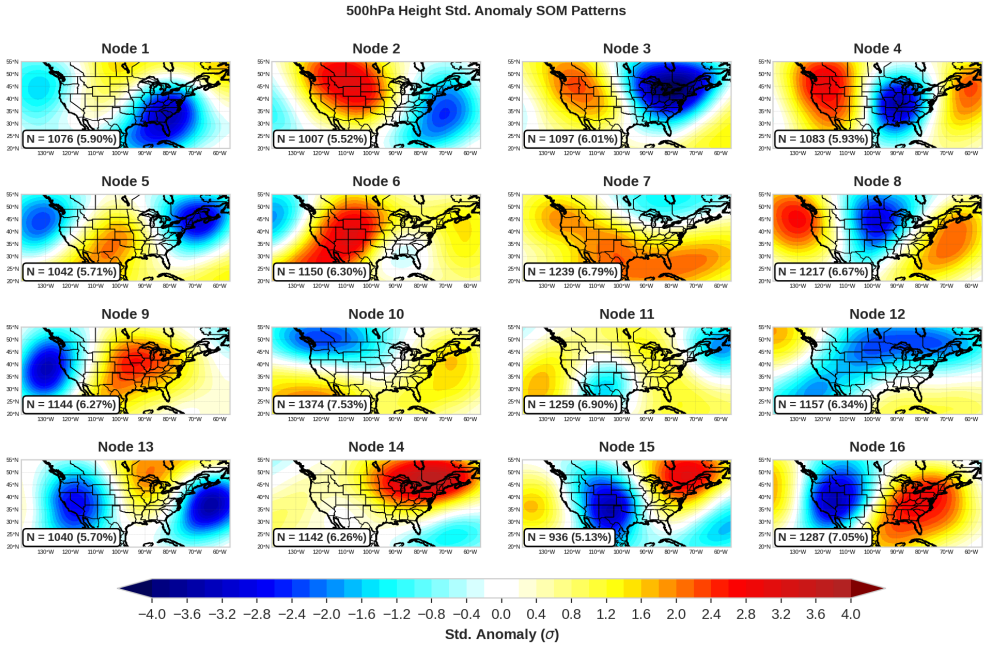

FIG. 1. The self-organizing map z500 standardized anomaly patterns. The positive height anomalies are shown in red and negative height anomalies are shown in blue.

(RCP) 4.5 and 8.5 are the two future scenarios that will be analyzed and are measured by the degree of radiative forcing that is estimated to be reached by 2100. RCP 4.5 describes a "moderate" forcing scenario with an increase of 4.5 W m^{-2} by 2100, which is a "peak and decay" scenario, with the highest radiative forcing occurring in 2040 and declining thereafter. RCP 8.5 describes a high-forcing scenario with an increase of 8.5 W m^{-2} by 2100.

To classify synoptic patterns, we use an artificial neural network called a self-organizing map (SOM). The SOM has become popular in synoptic climatology, since it is able to classify similar patterns together without the need for the user to "teach" the algorithm prior to clustering. The mapping of a SOM is realized in such a way that similar "nodes" are closer to one another and dissimilar nodes are far apart, with the most distinct lying on opposite sides of the map. A limitation to this approach requires that the number of clusters must be selected beforehand (Sheridan and Lee 2011). However, this is common among other clustering methods, including K-means clustering.

The self-organizing map is trained using daily mean 500 hPa geopotential height (z500) from the European Center for Medium-Range Weather Forecasting Reanalysis v5 (ERA5) for the years 1950–2020. A 31-day centered mean is calculated on the z500 data, explicitly, every day of the year (365 days) has a mean corresponding to 15 days prior and 15 days after to account for daily variations. A 30-year rolling mean is calculated on the centered means to serve as a climatological baseline. Standardized anomalies are computed for and used as input in the SOM. The node configuration in the SOM is organized as a 4×4 array to produce 16 nodes, with each node representing a different z500 standardized anomaly pattern. The trained SOM model is then applied to the historical and future simulations in order to provide a classification for each day. Convective parameters (e.g., CAPE, S06, CIN) are computed from CM3 simulations. Geopotential heights are computed on the hybrid-sigma coordinates via the hypsometric equation, and z500 is found by interpolation to 500 hPa.

To identify a potential severe weather day, the product of CAPE and S06 has shown to be a good parameter for when environments are favorable for SCS (Brooks et al. 2003). We will use the definition as in Hoogewind et al. (2017), where CAPE×S06 exceeds a threshold of 20,000 m^3 s^{-3}, given CAPE $\geq$ 100 J kg^{-1}, S06 $\geq$ 5 m s^{-1}, and CIN $\geq$ -100 J kg^{-1}. A potential severe weather is identified if the threshold is met or exceeded anytime between 12–12Z, and the number of days of severe weather (NDSEV) and be aggregated. CAPE and CIN are computed using a 100 hPa mixed-layer parcel.

3. Results

The 16 general synoptic patterns identified by the SOM, as illustrated by its component planes, are illustrated in Figure 1. In the top-left corner, patterns have positive

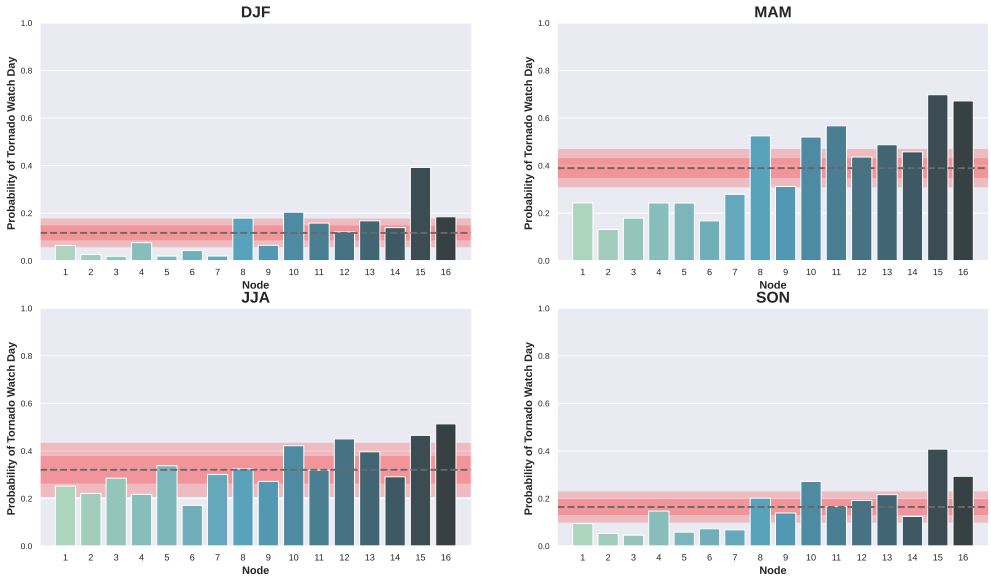

FIG. 2. The probability of a tornado watch given node. The dashed horizontal line represents the climatological daily mean probability of a tornado watch during the season. The light and red shading indicate 1 and 0.5 standard deviations (σ) from the mean, respectively.

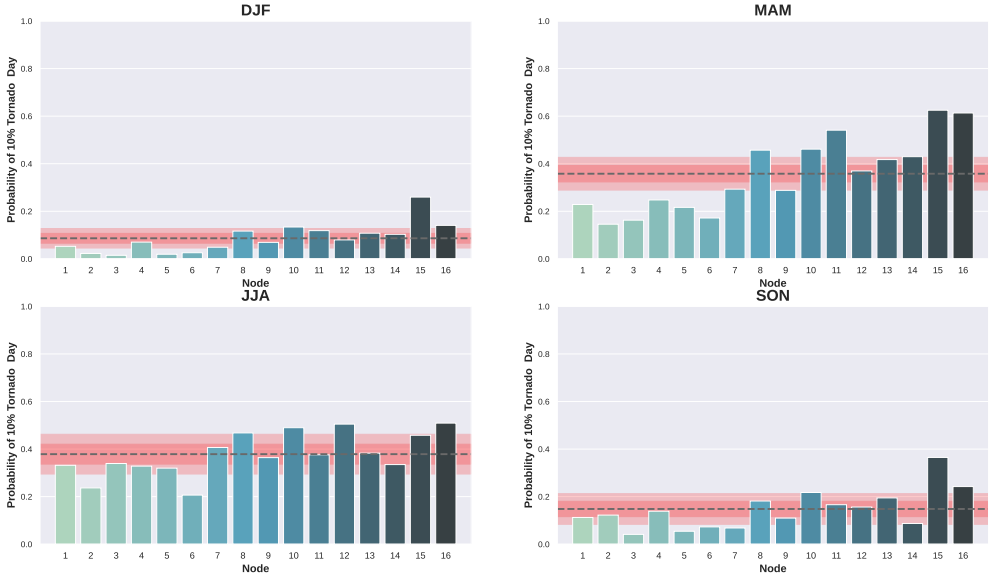

FIG. 3. As in Fig. 2, except for 10% Tornado PPH days.

z500 standardized height anomalies located in the western/central portions of the U.S., indicating ridging patterns, whereas increasing node number toward the lower right corner demonstrates height anomalies in the western/central U.S., or troughing. Nodes closer to one another are more closely related pattern wise. To assess severe weather likelihood, specifically tornadoes, each node is related to tornado watches and 10% tornado Practically Perfect Hindcast (PPH) days (Gensini et al. 2020) occurring during the period 1979–2020. The seasonal probability of a tornado watch day, given node, is assessed relative to climatology. Tornado watches are chosen because they are issued when environmental conditions are favorable for tornadoes. A node is more favorable if the probability of a tornado watch in a node exceeds the climatological daily probability for that season (and more so if the probability exceeds 0.5 or 1 standard deviations from the mean), and a node is unfavorable if falls below the climatological

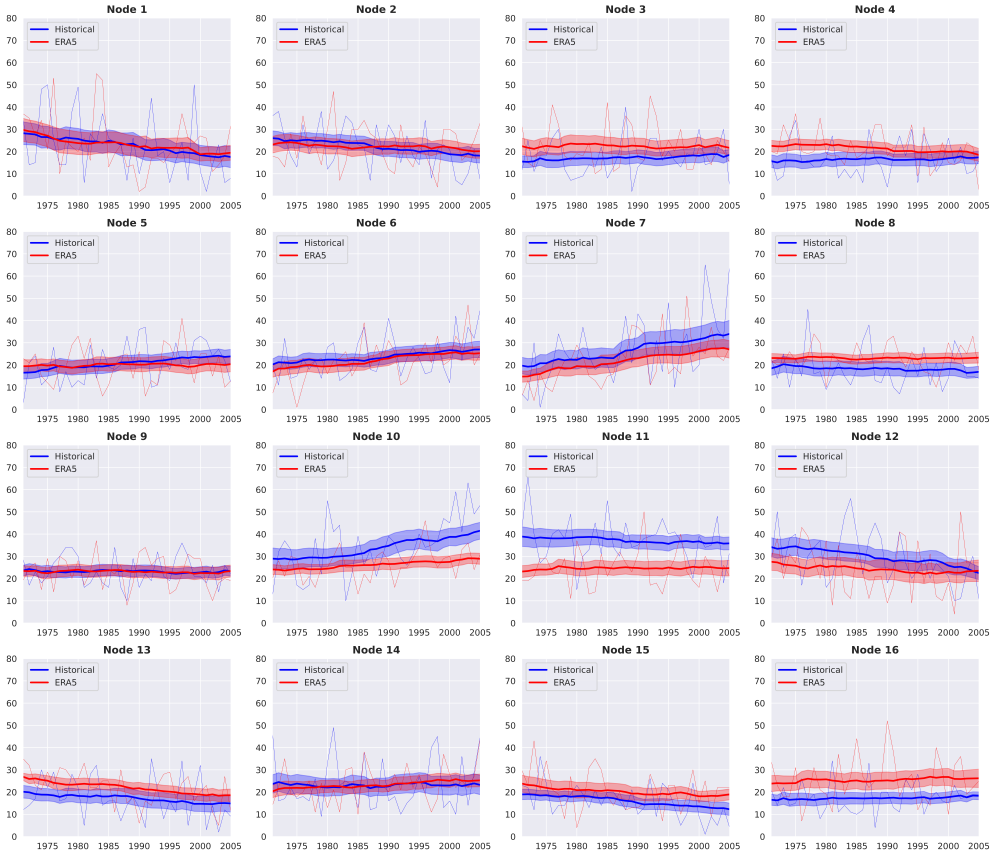

FIG. 4. Comparison of historical simulation (blue) and ERA5 reanalysis (red) on node frequency for the years 1971–2005. Shading indicates 95% confidence intervals.

daily mean. The results show that generally, more tornado watches are likely to occur on days where the node patterns from 8–16 are present (Fig. 2), this can be seen again with the 10% tornado PPH days (Fig. 3) for all seasons. Nodes 1–7 show to be unfavorable for tornado watches, specifically node 6 during March-April-May (MAM) and June-July-August (JJA) season.

To assess whether the GFDL-CM3 historical simulations (1971-–2005) can reasonably recreate the climatology of node frequencies, the annual and seasonal time series are compared against ERA5, in which the SOM was trained. GFDL-CM3 historical simulation seems to capture the ERA5 reanalysis well annually (Fig. 4). Although for nodes 10 and 11, the historical simulation seems to slightly overestimate the node occurrence, and in node 16, the historical simulation shows slight negative bias in comparison to ERA5. The seasonal time series (not shown) describes a similar scenario for node 11 during the months of March-April-May (MAM), and for both nodes 10 and 11 during June-July-August (JJA), although node 16 is well reconstructed in the historical simulation for those two seasons.

The annual time series of node frequency for the GFDL-CM3 simulations (1971–2100) indicate substantial increases in nodes 6 and 7 (Fig. 5), most distinctly within the last half of the 21st century. Nodes 6 and 7 increase more under RCP8.5 relative to RCP4.5, most prominently in node 7. Other nodes demonstrate less change, if at all, although there is some differences between RCP4.5 and RCP8.5 in nodes 1, 12, and 13. In these patterns, the frequency increases in RCP4.5 after 2040, while node 10, on the other hand, begins to increase again after 2080 in the RCP8.5. The time series of node frequencies by season (not shown) illustrate that the increasing annual trend of nodes 6 and 7 in RCP4.5 and RCP8.5 arise primarily during JJA, although node 7 frequency is significantly higher than node 6.

As the change in node frequencies are most notable by the late century, we limit the rest of our analyses for the period 2071–2100. On a seasonal basis, as illustrated in Fig. 6, DJF has slight increases in both simulations in southeast U.S.. During the spring (MAM), greater increases in NDSEV are noted in RCP8.5 relative to RCP4.5, most notably near Arkansas. During JJA there is a strong increase in the Northern Plains in both scenarios, with more pronounced

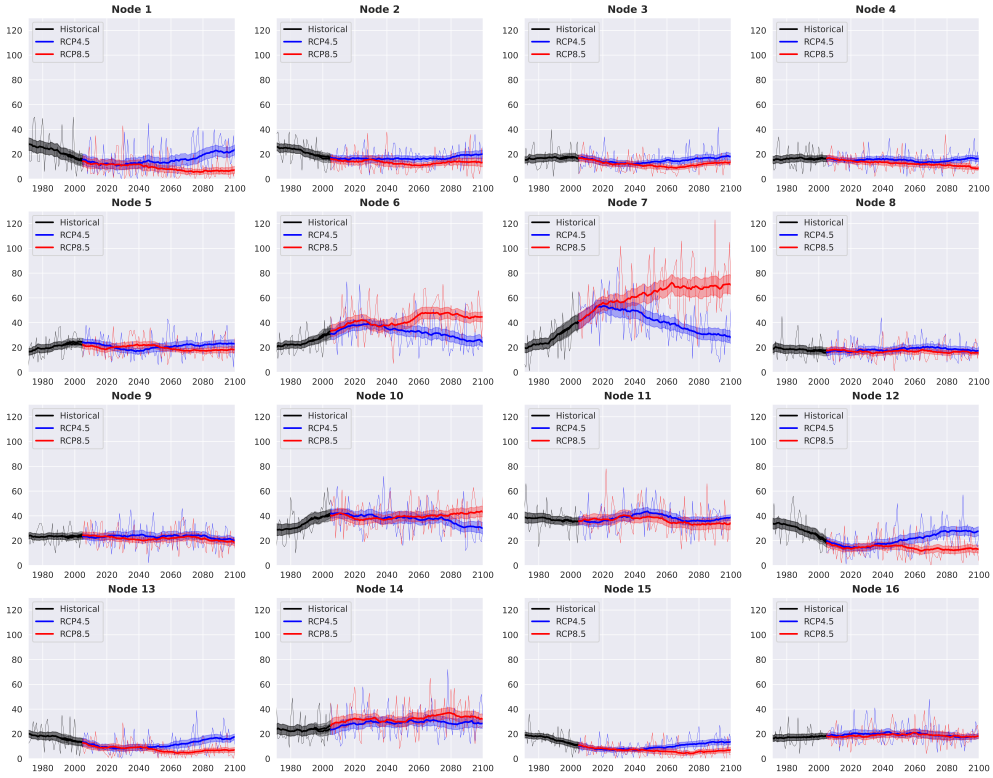

FIG. 5. Node frequency time series for historical simulation (black), RCP4.5 (blue), and RCP8.5 (red) from 1971-2100. Rolling 30-year means are denoted by the thicker lines and 95% confidence intervals are shaded.

changes in RCP8.5 ($\geq$ 15–20 days). However, RCP8.5 notices a slight decrease in NDSEV in the central Plains near the Texas Panhandle. For SON, there is smaller, yet statistically significant changes, in NDSEV for both RCP4.5 and RCP8.5. Because the most noted changes occur during JJA and in RCP8.5, we focus on those months and simulation when looking at differences in NDSEV by node (Fig. 7). Nodes 6, 7, and 14 have the most notable mean increases in NDSEV frequency, while nodes 1, 12, 13, and 15 show the most notable decreases for a large part of the country. For the latter, the decreases in 1, 12, and 13 occur due to a significant decrease in the pattern frequency from the historical. It becomes apparent that node 6 and 7 contribute the majority of the seasonal increases in NDSEV as a whole. Node 7 has a greater increase than node 6, where the highest change occurs in the Northern Plains.

Breaking down the individual parameter components of NDSEV, we will focus on changes in CAPE, S06, and CIN for RCP8.5 during JJA. CAPE increases in all nodes for JJA (Fig. 8), but node 6 and 7 have the highest increase in the northern Plains, with the highest magnitude in Nebraska. S06 decreases in all nodes for JJA (Fig. 9), however, nodes 6 and 7 see the most S06 decrease for the East coast and Midwest regions, and a very slight increase in Southern Texas. CIN increases for most nodes (Fig. 10), although there are some decreases that vary regionally in certain nodes (node 1 and 12). Node 6 and 7 increase in mean CIN all throughout the U.S., with the highest CIN magnitude increases located in the central CONUS. In node 7, the change in mean CIN magnitude is greatest in the Texas panhandle.

4. Discussion and Conclusions

Synoptic pattern analysis is useful for identifying favorable/unfavorable large-scale setups for SCS events, and by combining this analysis with environmental parameters it allows for assessment of synoptic pattern contribution to overall changes in severe weather days/ingredients. Our pattern approach is rather simple, based only on z500 standardized anomalies. For a more complete synoptic approach, other variables could also be taken into account when analyzing the patterns that are favorable, such as temperature, geopotential heights, and winds at varying pressure levels, mean sea-level pressure, low-level thermodynamic variables, to name a few, that might contribute to a more detailed pattern identification. The synoptic pattern and environment are not wholly independent. Troughs can alter the downstream atmosphere through differential temperature and moisture advection, which modifies lapse rates and impacts CAPE and CIN, and

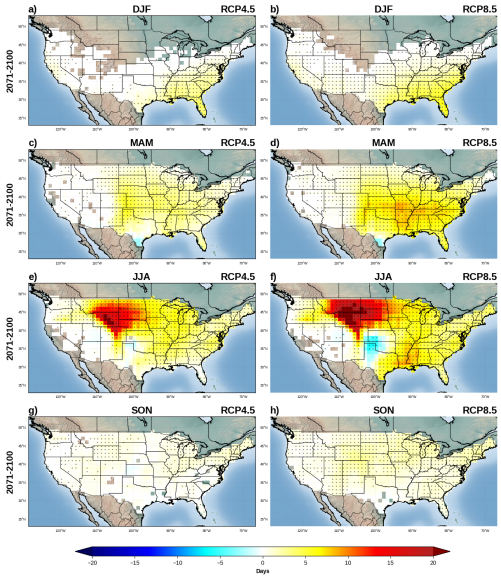

FIG. 6. Seasonal mean changes in NDSEV for RCP4.5 and RCP8.5 (2071–2100) relative to the historical climatology (1971–2000). Stippling indicate where the future and historical distributions are statistically significantly different at the 95% confidence level using the Mann-Whitney U-test.

thus preconditions the atmosphere for deep convection. Nonetheless, combining the two approaches still adds additional information not obtained from the environmental approach alone.

The increase in ridging patterns (nodes 6 and 7) in future projections is significant, particularly during the summer and in the RCP8.5 scenario. Node 6 and 7 patterns in the U.S. are generally less favorable for severe weather as a whole, but varies regionally. For example, during the summer, ridging patterns are supportive of severe weather along the northern periphery of the ridge, a so-called "ring of fire" pattern, while generally hostile to convection development beneath the interior of the ridge. Despite this, analysis demonstrates increases in NDSEV everywhere east of the Continental Divide, including the central Plains, despite an otherwise unfavorable pattern. This inconsistency in signal may arise in the environmental approach largely due to increasing CAPE. In comparison to the seasonal mean

For the period 2071–2100, the seasonal mean differences in NDSEV for RCP8.5, relative to the historical simulations, indicate that NDSEV are projected to increase overall in the north Central Plains. However, the Central Plains has a negative difference, which could be explained by decrease S06 or increase in CIN. The difference of NDSEV for node 7, however, does not see decreases in days, in fact, NDSEV, there is an overall increase which may be attributed to very high increases of CAPE in this pattern. CAPE has been shown to increase in previous environmental approach studies (e.g., Diffenbaugh et al. 2013) while S06 decreases, and the results of this study agree with that. Furthermore, the results indicate that no matter the pattern classification, CAPE increases, suggesting that anthropogenic forcing, and resultant warming, contribute to increasing CAPE. Although the S06 decreases in many of the node patterns, that is not the consistent for all node patterns and regional variations exist.

Hoogewind et al. (2017) found that CIN increases strongly during JJA in the central U.S. in 2071–2100, and this study found that CIN increased in nearly all patterns during JJA, with exception for regional decreases in nodes 1, 12, and 15. Many areas of increase in nodes 4, 5, 8, and 16 were relatively large in terms of changes in the mean, but the seasonal distributions were not statistically significantly different.

This research combined the well-established environmental approach with a synoptic pattern analysis to investigate the potential change in severe weather within 21st century projections from GFDL-CM3. Using a self-organizing map, 16 common daily mean z500 standardized anomaly patterns were identified from ERA5 reanalysis; the trained SOM model was then used to classify patterns within GFDL-CM3 simulations. This study found that two western/central ridge patterns increased in frequency within RCP4.5 and RCP8.5, most notably in RCP8.5 for JJA. Evaluating mean changes in NDSEV, CAPE, S06, and CIN by node, CAPE and CIN consistently increase while S06 decrease overall, and the magnitude and location of the differences varied by pattern type.

Although not the first to examine synoptic climatology and severe thunderstorms (e.g., Johns 1984) or synoptic variability in a warming future climate (as in Lee 2012), this work shows that changes in environmental parameters are pattern dependent, implying that some environments will become more frequent than others depending on time of year and region. The use of only one GCM is a limitation of this study, whereas an ensemble approach would allow for assessment of possible trajectories and uncertainty in future projections, especially during JJA when GCMs tend to diverge (e.g., Diffenbaugh et al. 2013). Also, our synoptic patterns were defined by only using z500, where finding more synoptic variables associated with SCS environments (as in Lee 2012) would provide a greater profile on severe environment changes. In the future, this work will be expanded to incorporate the convection-allowing regional climate simulations of Hoogewind et al. (2017) which downscaled GFDL-CM3, to further examine the pattern-environment relationship with respect to simulated SCSs.

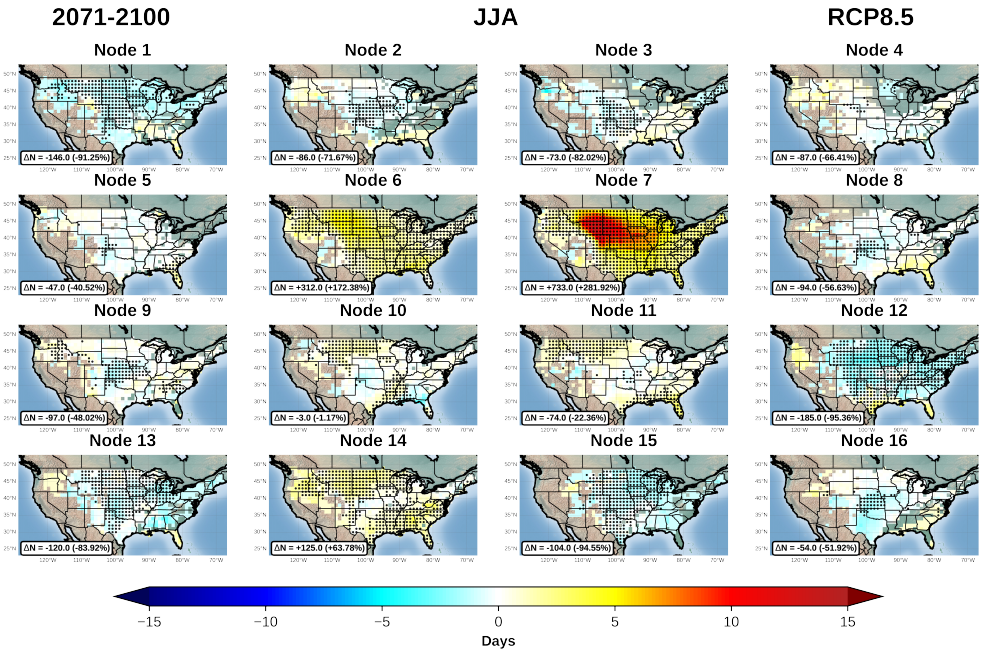

FIG. 7. Mean change in RCP8.5 JJA NDSEV (2071–2100) relative to the historical baseline (1971–2000). Stippling indicates where the future and historical distributions are statistically significantly different at the 95% confidence level using the Mann-Whitney U-test. Annotations in the lower-left corner of each panel indicate the change in total node frequency (and percentage change) between the future and historical periods.

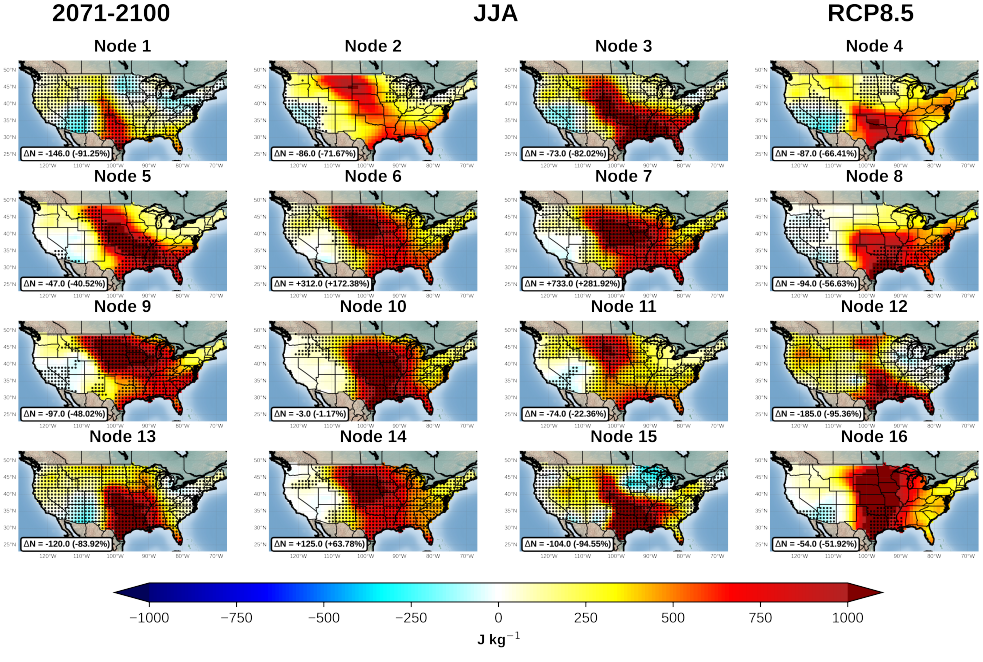

FIG. 8. As in Fig. 7, except for CAPE

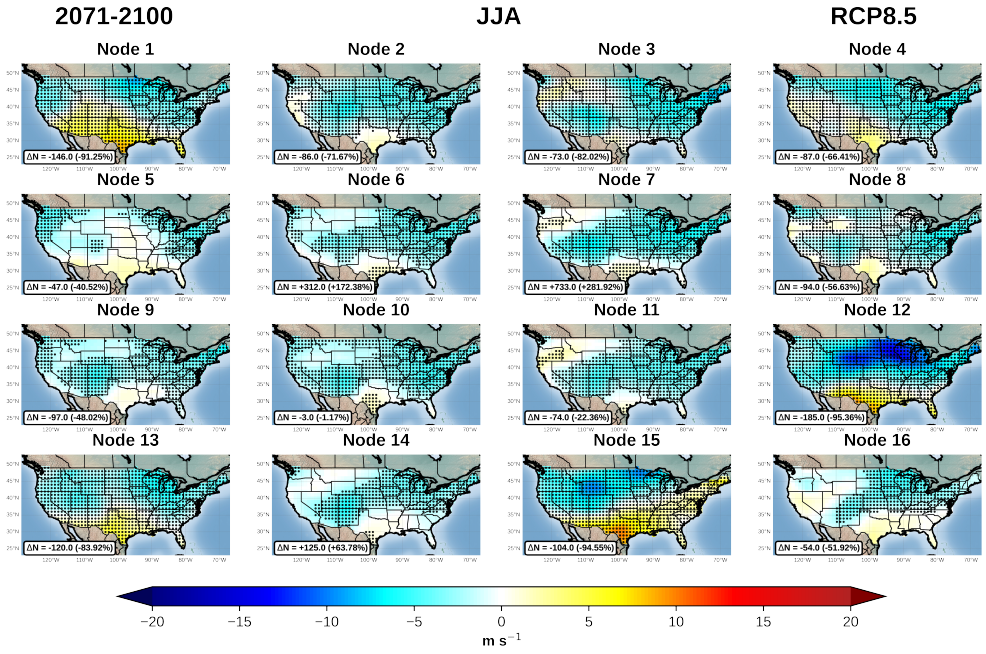

FIG. 9. As in Fig. 8, except for S06.

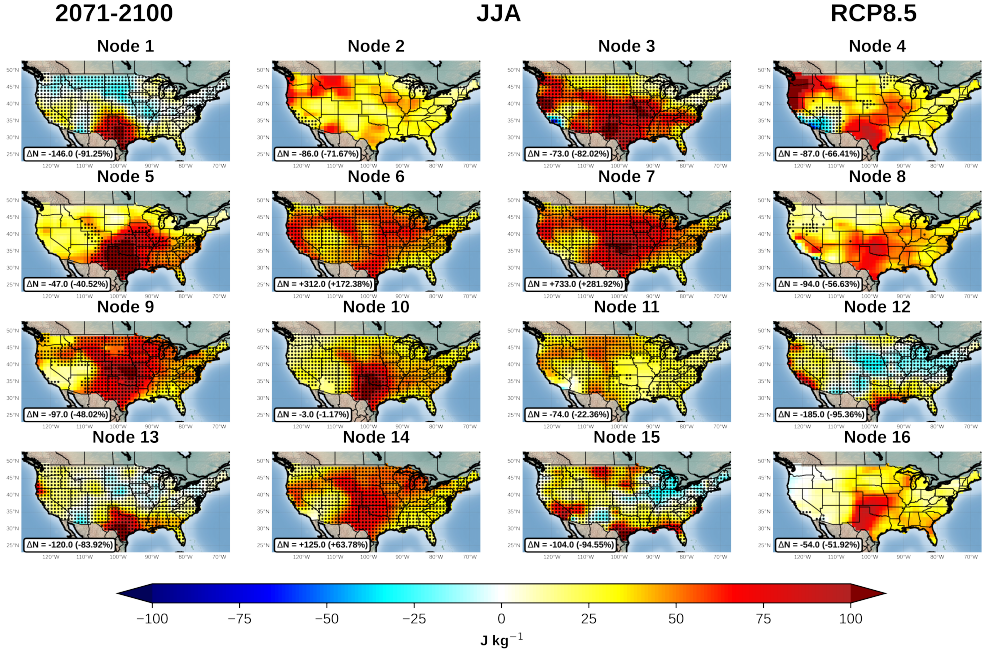

FIG. 10. As in Fig. 8, except for CIN.

Acknowledgments. We would like to thank Alex Marmo and Dr.Daphne LaDue for their incredible job at directing the first in-person NWC REU since 2019.

The corresponding author would like to give a very special thanks to Dr. Kimberly Hoogewind and Dr. Harold Brooks for their mentoring and indispensable insight on the topics in this research, also thank you Dr. Hoogewind for teaching me new ways to code.

This material is based upon work supported by the National Science Foundation under Grant No. AGS-1560419, and NOAA/Office of Oceanic and Atmospheric Research under NOAA-University of Oklahoma Cooperative Agreement #NA11OAR4320072, U.S. Department of Commerce. The statements, findings, conclusions, and recommendations are those of the author(s) and do not necessarily reflect the views of the National Science Foundation, NOAA, or the U.S. Department of Commerce.

References

Brooks, H. E., J. W. Lee, and J. P. Craven, 2003: The spatial distribution of severe thunderstorm and tornado environments from global reanalysis data. *Atmospheric Research*, **67-68**, 73–94, doi: https://doi.org/10.1016/S0169-8095(03)00045-0.

Chen, J., A. Dai, Y. Zhang, and K. L. Rasmussen, 2020: Changes in Convective Available Potential Energy and Convective Inhibition under Global Warming. *Journal of Climate*, **33 (6)**, 2025 – 2050, doi: 10.1175/JCLI-D-19-0461.1.

Diffenbaugh, N. S., M. Scherer, and R. J. Trapp, 2013: Robust increases in severe thunderstorm environments in response to greenhouse forcing. *Proceedings of the National Academy of Sciences*, **110 (41)**, 16 361–16 366, doi:10.1073/pnas.1307758110.

Gensini, V. A., A. M. Haberlie, and P. T. Marsh, 2020: Practically Perfect Hindcasts of Severe Convective Storms. *Bulletin of the American Meteorological Society*, **101 (8)**, E1259–E1278, doi:10.1175/BAMS-D-19-0321.1.

Gensini, V. A., and T. L. Mote, 2014: Estimations of Hazardous Convective Weather in the United States Using Dynamical Downscaling. *Journal of Climate*, **27 (17)**, 6581–6589, doi:10.1175/JCLI-D-13-00777.1.

Gensini, V. A., and T. L. Mote, 2015: Downscaled estimates of late 21st century severe weather from CCSM3. *Climatic Change*, **129 (1)**, 307–321, doi:10.1007/s10584-014-1320-z.

Hoogewind, K. A., M. E. Baldwin, and R. J. Trapp, 2017: The Impact of Climate Change on Hazardous Convective Weather in the United States: Insight from High-Resolution Dynamical Downscaling. *Journal of Climate*, **30 (24)**, 10 081–10 100, doi:10.1175/JCLI-D-16-0885.1.

Hope, P. K., 2006: Projected future changes in synoptic systems influencing southwest Western Australia. *Climate Dynamics*, **26 (7)**, 765–780, doi:10.1007/s00382-006-0116-x.

Johns, R. H., 1984: A Synoptic Climatology of Northwest-Flow Severe Weather Outbreaks. Part II: Meteorological Parameters and Synoptic Patterns. *Monthly Weather Review*, **112 (3)**, 449–464, doi:10.1175/1520-0493(1984)112⟨0449:ASCONF⟩2.0.CO;2.

Kunkel, K. E., and Coauthors, 2013: Monitoring and Understanding Trends in Extreme Storms: State of Knowledge. *Bulletin of the American Meteorological Society*, **94 (4)**, doi:10.1175/BAMS-D-11-00262.1.

Lee, C. C., 2012: Utilizing synoptic climatological methods to assess the impacts of climate change on future tornado-favorable environments. *Natural Hazards*, **62 (2)**, 325–343, doi:10.1007/s11069-011-9998-y.

NOAA, 2022: Noaa national centers for environmental information (ncei) u.s. billion-dollar weather and climate disasters (2022). doi: 10.25921/stkw-7w73.

Robinson, E. D., R. J. Trapp, and M. E. Baldwin, 2013: The Geospatial and Temporal Distributions of Severe Thunderstorms from High-Resolution Dynamical Downscaling. *Journal of Applied Meteorology and Climatology*, **52 (9)**, doi:10.1175/JAMC-D-12-0131.1.

Sheridan, S. C., and C. C. Lee, 2011: The self-organizing map in synoptic climatological research. *Progress in Physical Geography: Earth and Environment*, **35 (1)**, 109–119, doi:10.1177/0309133310397582, publisher: SAGE Publications Ltd.

Thompson, R. L., R. Edwards, J. A. Hart, K. L. Elmore, and P. Markowski, 2003: Close Proximity Soundings within Supercell Environments Obtained from the Rapid Update Cycle. *Weather and Forecasting*, **18 (6)**, 1243–1261, doi:10.1175/1520-0434(2003)018⟨1243:CPSWSE⟩2.0.CO;2.

Trapp, R. J., N. S. Diffenbaugh, H. E. Brooks, M. E. Baldwin, E. D. Robinson, and J. S. Pal, 2007: Changes in severe thunderstorm environment frequency during the 21st century caused by anthropogenically enhanced global radiative forcing. *Proceedings of the National Academy of Sciences*, **104 (50)**, 19 719–19 723, doi:10.1073/pnas.0705494104.

Trapp, R. J., E. D. Robinson, M. E. Baldwin, N. S. Diffenbaugh, and B. R. J. Schwedler, 2011: Regional climate of hazardous convective weather through high-resolution dynamical downscaling. *Climate Dynamics*, **37 (3)**, 677–688, doi:10.1007/s00382-010-0826-y.